

# Collinear Four-Wave Mixing of Two-Component Matter Waves

Daniel Pertot,<sup>\*</sup> Bryce Gadway, and Dominik Schneble

Department of Physics and Astronomy, Stony Brook University, Stony Brook, New York 11794-3800, USA

(Dated: November 8, 2018)

We demonstrate atomic four-wave mixing of two-component matter waves in a collinear geometry. Starting from a single-species Bose–Einstein condensate, seed and pump modes are prepared through microwave state transfer and state-selective Kapitza–Dirac diffraction. Four-wave mixing then populates the initially empty output modes. Simulations based on a coupled-mode expansion of the Gross–Pitaevskii equation are in very good agreement with the experimental data. We show that four-wave mixing can play an important role in studies of bosonic mixtures in optical lattices. Moreover our system should be of interest in the context of quantum atom optics.

PACS numbers: 03.75.Mn, 03.75.Gg, 67.85.Hj

Four-wave mixing is a fundamental, well-studied concept in nonlinear optics and spectroscopy [1]. Its matter-wave analogue, based on binary collisions in ultracold atomic gases, was first demonstrated experimentally a decade ago [2, 3], establishing the field of nonlinear atom optics [4]. In four-wave mixing (FWM), two waves form a grating from which a third wave diffracts, thus generating a fourth wave. This process has been used for coherent matter-wave amplification [5], and for the generation of correlated atom pairs [4–7]. Energy and momentum conservation require the magnitudes of all atomic momenta in the center-of-mass frame to be equal which, for atoms in a single internal state, necessitates a two-dimensional geometry [3]. By modifying the dispersion relation with an optical lattice, nondegenerate FWM of a single species becomes possible also in one dimension [8].

Despite considerable theoretical work on atomic FWM with more than one internal state [9–11], experiments have only very recently started to explore possible mechanisms for such FWM [7, 12]. The additional internal degree of freedom allows for degenerate FWM to occur in one dimension, with pairs of waves in different internal states sharing the same momentum mode, opening up possibilities to generate nonclassical matter-wave states, e.g. with macroscopic spin entanglement [10]. In this Letter, we demonstrate free-space collinear atomic FWM involving two internal states with distinct, macroscopically populated momentum modes.

Apart from the relevance for quantum atom optics, another important context arises in experimental studies of bosonic mixtures in optical lattices [13–15]. These systems are of high interest not only in connection with applications to quantum magnetism [16], but also for studies of decoherence mechanisms [17], and for lattice thermometry [14, 15]. Most experiments with ultracold atoms in optical lattices to date rely on time-of-flight information. In particular, a sudden release from the lattice projects the band populations onto plane-wave states [18]. We find that for a homonuclear mixture of interacting superfluids, FWM processes can alter the expected momentum-space distributions, masking or even

mimicking *in situ* interaction effects.

In order to induce collinear two-component FWM, we apply a state-selective optical lattice pulse to a Bose–Einstein condensate containing atoms in two internal states  $|a\rangle$  and  $|b\rangle$ , as illustrated in Fig. 1 (A). The pulse induces Kapitza–Dirac (KD) diffraction [19, 20] producing recoiling  $|a\rangle$  atoms in both positive and negative momentum modes  $|\pm 2\rangle \equiv |\pm 2\hbar k_L\rangle$  where  $k_L = 2\pi/\lambda_L$ , while the  $|b\rangle$  atoms remain unaffected. Subsequently, as illustrated in Fig. 1 (B), the  $|b\rangle$  atoms Bragg diffract from the density modulation formed by the interference of the recoiling  $|a\rangle$  atoms  $|a, 2\rangle \equiv |a\rangle \otimes |2\rangle$  with those at rest,  $|a, 0\rangle$ . Because of momentum exchange collisions, the recoiling  $|a\rangle$  atoms are coherently transferred back into  $|0\rangle$ , as recoiling atoms  $|b, 2\rangle$  are produced. This process is formally not distinguishable from coherent (pseudo-) spin exchange. Our system might thus pose an interesting alternative to spinor condensates for the creation of nonclassical states [10, 12]. We note that due to the symmetry of the KD pulse, another, independent “copy” of the FWM process occurs on the negative momentum side. For quantum atom optics purposes, this can easily be avoided by using a state-selective Bragg pulse instead, which also allows for extended control of the initial mode populations. In the present work, however, we are con-

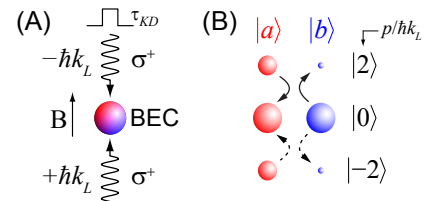


FIG. 1. Experimental scheme. (A) State-selective Kapitza–Dirac diffraction of a two-component Bose–Einstein condensate. (B) Four-wave mixing (solid arrows) with pump modes  $|b, 0\rangle$ ,  $|a, 2\rangle$  and seed mode  $|a, 0\rangle$  transfers  $|b\rangle$  atoms to the output mode  $|b, 2\rangle$ . Because of the symmetry of the problem, the process also occurs for the modes  $|a, -2\rangle$  and  $|b, -2\rangle$  (dashed arrows).

tent with applying a KD pulse, mainly out of technical convenience.

Our experimental setup has been described in detail in Ref. [21]. In a crossed-beam optical dipole trap at 1064 nm wavelength, we produce nearly pure  $^{87}\text{Rb}$  Bose–Einstein condensates in the  $|a\rangle \equiv |F=1, m_F=-1\rangle$  hyperfine state typically containing about  $1.6 \times 10^5$  atoms. The trap is approximately isotropic with a mean trap frequency around 50 Hz and an alignment-dependent vertical frequency  $\omega_z/2\pi$  between 40 and 50 Hz. Immediately after a variable fraction of the condensate is transferred into the state  $|b\rangle \equiv |2, -2\rangle$  via a microwave Landau–Zener sweep [22], a state-selective lattice beam [23] at  $\lambda_L = 785.1$  nm is pulsed on along the vertical  $z$  direction ( $1/e^2$  radius 230  $\mu\text{m}$ ) for a time  $\tau_{KD}$ . The polarization ( $\sigma^+$ ) is chosen such that only the  $|a\rangle$  atoms feel the optical lattice potential formed through retro-reflection of the beam. A magnetic field ( $\sim 0.4$  G) along the beam axis defines the quantization axis. After release from the trap and a few milliseconds of free evolution, during which the FWM occurs, a magnetic field gradient (Stern–Gerlach pulse) spatially separates the two hyperfine states along the horizontal  $x$  axis for detection. The atoms are imaged after a total time of flight of 15 ms via near-resonant absorption imaging by a 100  $\mu\text{s}$  long pulse of  $F=2 \rightarrow F'=3$  imaging light, combined with  $F=1 \rightarrow F'=2$  repumping light, which ensures equal detection efficiencies for both hyperfine states.

In Fig. 2, typical absorption images are shown for three different fractions of  $|a\rangle$  atoms  $f_a \equiv N_a/N$ . The KD pulse duration (25  $\mu\text{s}$ ) and the lattice depth  $V_a$  for atoms of type  $|a\rangle$  ( $6 E_R$ , where  $E_R = \hbar^2 k_L^2/2m$  is the recoil energy), are chosen such that half of the  $|a\rangle$  population is diffracted into  $|\pm 2\rangle$ , while higher orders remain largely unpopulated. By analyzing single-component diffraction patterns [20], we have determined the lattice depths for each component, confirming that atoms of type  $|b\rangle$  experience  $< 5\%$  of the lattice depth seen by the  $|a\rangle$  atoms. On their own, the  $|b\rangle$  atoms therefore are not affected

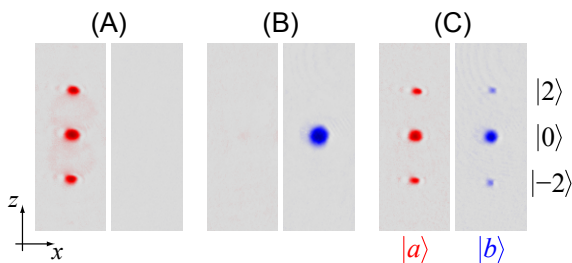


FIG. 2. Typical absorption images taken after application of the state-selective Kapitza–Dirac pulse ( $\tau_{KD} = 25 \mu\text{s}$ ,  $V_a = 6 E_R$ ), 15 ms time of flight and Stern–Gerlach separation along  $x$ , for the case of (A) only  $|a\rangle$  atoms present ( $f_a = 1$ ), (B) only  $|b\rangle$  atoms ( $f_a = 0$ ), and (C) equal populations of both components ( $f_a = 0.5$ ).

by the lattice pulse, as shown in Fig. 2 (B). However, when both components are present, a significant fraction of  $|b\rangle$  atoms is transferred into the  $|\pm 2\rangle$  momentum modes [Fig. 2 (C)].

We have measured the amount of diffracted atoms in each state as a function of  $f_a$ . As shown in Fig. 3 (A), the fraction of diffracted  $|b\rangle$  atoms  $(N_{b,+2} + N_{b,-2})/N_b$  monotonically increases from zero towards a maximum as  $f_a$  is increased, consistent with the picture that the grating formed by interference of the  $|a, 0\rangle$  and  $|a, \pm 2\rangle$  modes, from which the atoms in  $|b, 0\rangle$  diffract, gets deeper as the number of  $|a\rangle$  atoms grows. The relative number of diffracted  $|a\rangle$  atoms has a pronounced minimum near  $f_a = 0.5$ , which can be interpreted as a “backaction” of the  $|b\rangle$  atoms onto the  $|a\rangle$  grating.

To obtain a more quantitative understanding, we theoretically model our system starting from the coupled Gross–Pitaevskii equations (GPE) for the order parameters  $\Phi_\alpha(\mathbf{r}, t)$  of the two components  $\alpha \in \{a, b\}$

$$i\hbar \partial_t \Phi_\alpha = \left( -\frac{\hbar^2}{2m} \nabla^2 + V_\alpha^{\text{tot}} + \sum_{\beta \in \{a, b\}} g_{\alpha\beta} |\Phi_\beta|^2 \right) \Phi_\alpha, \quad (1)$$

where  $g_{\alpha\beta} = 4\pi\hbar^2 a_{\alpha\beta}/m$ ,  $m$  is the atomic mass, and the intra and interspecies  $s$ -wave scattering lengths  $a_{aa}$ ,  $a_{bb}$ , and  $a_{ab}$  in units of  $a_0$  are 100.4, 99.0, and 99.0, respectively [24]. The trapping and lattice potentials are given by  $V_\alpha^{\text{tot}} = V_{\text{trap}}(\mathbf{r}, t) + V_\alpha(t) \sin^2(k_L z)$ . Similar to the slowly varying envelope approximation (SVEA) [3, 11], we approximate the solution of Eq. (1) as an expansion in terms of momentum modes, or wave packets, moving along  $z$  with multiples of the recoil velocity  $v_R = \hbar k_L/m$

$$\Phi_\alpha(\mathbf{r}, t) = \sum_{n=-\infty}^{\infty} c_{n\alpha}(t) e^{ink_L z} \Phi_0(\mathbf{r} - \hat{z} n v_R t, t). \quad (2)$$

We further assume that the wave packets  $\Phi_0$  are of Thomas–Fermi form and that they expand hydrodynamically after release from the trap [25], which leads to a significant simplification compared to a full SVEA simulation. On the time scales of interest, phase-separation [26] can be neglected, and we have  $\Phi_\alpha \propto \Phi_0$  for both components just after the microwave transfer [26]. Since the momentum spread of  $\Phi_0$  is much less than  $\hbar k_L$ , the modes in the expansion are quasi-orthogonal. After inserting the ansatz (2) into Eq. (1), we arrive at a system of coupled equations for the amplitudes  $a_n(t) \equiv c_{na}(t)$

$$i\hbar \partial_t a_n = E_R n^2 a_n + V_a(t) \left[ \frac{1}{2} a_n - \frac{1}{4} (a_{n+2} + a_{n-2}) \right] + \sum_{mm'n'} (g_{aa} a_m^* a_{m'} + g_{ab} b_m^* b_{m'}) a_{n'} h_{nmm'n'}(t)$$

and similarly for the other component  $b_n(t) \equiv c_{nb}(t)$ . Here,  $h_{nmm'n'}(t) \propto \delta(n+m-m'-n')$  denotes overlap integrals that include the effective temporal decay of the

nonlinear interaction, as the different wave packets separate, and as the density decreases during the expansion. The terms responsible for FWM are of the form  $b_m^* b_n a_m$  (and  $a_m^* a_n b_m$  for the  $|b\rangle$  component) with  $m \neq n$ . After adjacent modes ( $|m - n| = 2$ ), for which the overlap decays the slowest, have completely separated, the populations remain frozen, since only equal-momentum self and cross-phase modulation terms of the forms  $|a_n|^2 a_n$  and  $|b_n|^2 a_n$  survive. With a typical Thomas–Fermi radius  $R_z \sim 10 \mu\text{m}$ , we obtain a typical separation time  $t_{\text{sep}} \approx 2R_z/2v_R$  of 1.7 ms.

The full set of observed populations  $|a_n|^2$  and  $|b_n|^2$  after FWM is plotted in Fig. 3 (B), along with predictions of our model obtained with parameters according to the experimental ones, leaving only the total atom number  $N$  as a fit parameter. The overall agreement between data and theory is remarkable. The maximum FWM yield occurs near  $f_a = 2/3$  where the initial populations of the pump and seed modes are equal, maximizing the FWM term  $a_m^* a_n b_m$  at  $t = 0$  [3]. The data also clearly show the correlated growth of  $|b_{\pm 2}|^2$  and  $|a_0|^2$ , along with a corresponding depletion of the pump modes  $|b_0|^2$  and  $|a_{\pm 2}|^2$ , as detailed in the inset.

We note that since the FWM yield is proportional to the interspecies scattering length as well as to the overlap  $\int d\mathbf{r} |\Phi_a|^2 |\Phi_b|^2$  of the two components, it can serve as a sensitive probe for both quantities. As a practical example, we use two-component FWM as a clear “single-shot” diagnostic for the optimization of component overlap. By carefully canceling magnetic field gradients, we are able to sustain overlap, i.e. FWM yield, for up to 2 s after the microwave transfer.

To further confirm the coherence of the observed two-component FWM as implied by our model, we directly map out the time evolution of the output mode population  $|b_{\pm 2}|^2$  by interrupting the FWM process after a variable time through the selective removal of  $|a\rangle$  atoms with a  $50 \mu\text{s}$  long “blast” pulse of repumping light. As shown in Fig. 3 (C), the atom number in the  $|b, \pm 2\rangle$  modes smoothly grows from zero to a maximum value reached around the expected separation time. The nonlinear, initially quadratic growth is indicative of a coherent process [3, 5] (other signs would be an overshoot and oscillations, which however would require higher densities or longer overlap). To exclude the possibility that the observed growth is merely an artifact caused by density-dependent losses of  $|b\rangle$  atoms accompanying the blast (due to collisions with  $|a\rangle$  atoms), we repeat the experiment with the polarization of the lattice beam chosen such that both components experience the same lattice depth of about  $6 E_R$ . In this case, we expect the  $|b, \pm 2\rangle$  modes to be populated immediately after the KD pulse, as indeed can be seen in Fig. 3 (C). Further, no FWM is expected to occur for  $V_b = V_a$ , as the internal and external state dynamics are decoupled. By comparing the observed time evolution for this reference case with the

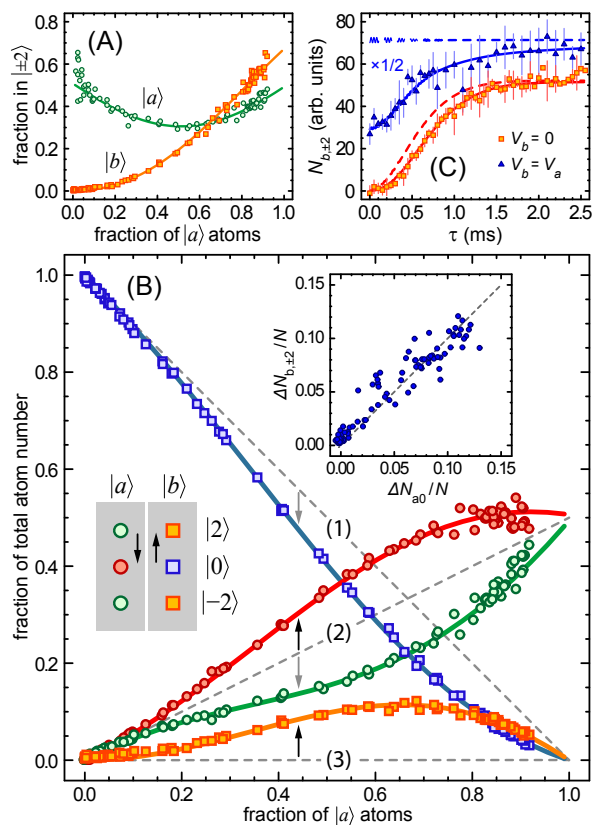


FIG. 3. Mode populations after four-wave mixing. (A) Fraction of atoms with momenta  $\pm 2\hbar k_L$  in state  $|a\rangle$  (green circles) and  $|b\rangle$  (orange squares). (B) Populations  $|c_{n\alpha}|^2 = N_{n\alpha}/N$  of the modes  $|a, n\rangle$ , as indicated in the plaquette. The dashed lines (1), (2), and (3) indicate the initial conditions before FWM,  $|b_0(0)|^2$ ,  $|a_0(0)|^2 = |a_{\pm 2}(0)|^2$ , and  $|b_{\pm 2}(0)|^2$  (where  $\pm 2$  indicates the combined populations). The arrows indicate the temporal evolution of the populations. The solid lines represent the predictions of the model ( $V_a = 5.6 E_R$ ,  $\tau_{KD} = 25 \mu\text{s}$ ,  $\omega_z = 2\pi \times 51 \text{ Hz}$ ,  $N = 1.4 \times 10^5$ ). The inset shows the transferred  $|b\rangle$  population vs the transferred  $|a\rangle$  population, where the dashed line represents a slope of unity. (C) Growth of the population in  $|b, \pm 2\rangle$  following the Kapitza–Dirac pulse for  $V_b = 0$  (orange squares) and for  $V_b = V_a$  (blue triangles,  $\times 1/2$ ). The FWM was interrupted after a variable time  $\tau$  by blasting away the  $|a\rangle$  atoms. Each data point is averaged over 2–6 runs (here  $\omega_z = 2\pi \times 41 \text{ Hz}$ ,  $f_a = 0.5$ ). The dashed lines are the predictions of the uncorrected model (including higher order FWM terms), whereas the solid lines take into account the loss of atoms during the blasting process (see text). The blast-loss model was calibrated by fitting to the  $V_b = V_a$  data.

expected one, we can calibrate our model for the blast-induced losses, which assumes a relative loss of  $|b\rangle$  atoms proportional to the density of  $|a\rangle$  atoms in the overlap region. With this correction, the theoretical time evolution for  $V_b = 0$  matches the experimental data very well.

So far, we have discussed controlled FWM after application of a short optical pulse to induce diffraction. Now, we turn to the question whether FWM is also rele-

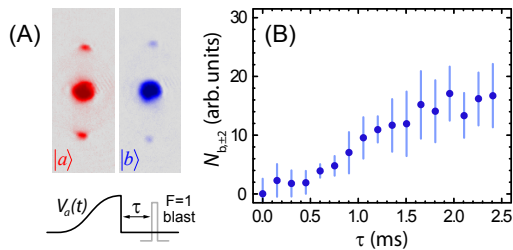


FIG. 4. Four-wave mixing effects for an adiabatically ramped-up optical lattice. (A) An  $|a\rangle$ -selective lattice is ramped up to a depth of  $6.0 E_R$  within 100 ms onto an equal mixture ( $f_a = 0.5$ ). After release and 17 ms time of flight,  $|b\rangle$  atoms appear in  $|\pm 2\rangle$ . (B) Growth of population in  $|b, \pm 2\rangle$  as determined by blasting away the  $|a\rangle$  atoms after an evolution time  $\tau$ . Each data point is averaged over 6 runs.

vant for adiabatically ramped-up, state-selective optical lattices. For such a system, interspecies interactions can be expected to give rise to diffraction effects qualitatively similar to those due to FWM. The density profile of the  $|a\rangle$  component gets spatially modulated by the optical lattice, thus forming an “atomic lattice” that, in turn, should modulate the density of the  $|b\rangle$  component, leading to diffraction peaks at  $\pm 2\hbar k_L$  immediately after release. However, we find that, at least as long as both components are in the superfluid state, FWM is by far the dominant mechanism for the emergence of recoiling  $|b\rangle$  atoms, caused by the projection of the  $|a\rangle$  component into plane-wave momentum modes after release. We note that the mismatch between the dispersion relations for  $|a\rangle$  and  $|b\rangle$  atoms suppresses FWM while the lattice is on. For  $f_a = 0.5$  and  $V_a = 6 E_R$  ( $V_b = 0$ ), as shown in Fig. 4 (A), we measure a relative population of up to 1.5 % in each of the  $|b, \pm 2\rangle$  states. Assuming this to be caused by a density modulation would require an atomic lattice modulation depth of  $2 E_R$ , more than the chemical potential of the condensate in the lattice. A blast measurement as discussed above shows that the population in the observed peaks slowly grows only after release from the lattice [Fig. 4 (B)], indicating that the peaks are indeed caused by FWM.

We have performed analogous experiments for different final lattice depths  $V_a$ , and with additional, state-independent lattices along the  $x$  and  $y$  directions. These results will be presented in detail in a future publication. In brief, we observe similar FWM effects along the state-dependent axis (cf. also [15], Fig. 8); however, we find that no FWM peaks are produced when the  $|a\rangle$  atoms are in the Mott regime. This is consistent with the notion that FWM as described relies on the existence of a well-defined macroscopic phase and thus bears the potential to be used as a sensitive probe of phase coherence.

To summarize, we have demonstrated collinear four-

wave mixing in a two-component mixture of bosonic atoms, and find excellent agreement with a simple theoretical model. Our work is of relevance both in the context of quantum atom optics, and for experimental studies of bosonic mixtures in optical lattices.

We thank R. Reimann for experimental contributions and T. Bergeman for careful reading of the manuscript. This work was supported by NSF (PHY-0855643), ONR (DURIP), the Research Foundation of SUNY, and through the GAANN program (B.G.) of the US ED.

\* dpertot@ic.sunysb.edu

- [1] R. W. Boyd, *Nonlinear Optics* (Academic Press, San Diego, 2003).
- [2] L. Deng *et al.*, *Nature* **398**, 218 (1999).
- [3] M. Trippenbach, Y. B. Band, and P. S. Julienne, *Opt. Express* **3**, 530 (1998); *Phys. Rev. A* **62**, 023608 (2000).
- [4] P. Meystre, *Atom Optics* (Springer, New York, 2001).
- [5] J. M. Vogels, K. Xu, and W. Ketterle, *Phys. Rev. Lett.* **89**, 020401 (2002); J. M. Vogels, J. K. Chin, and W. Ketterle, *ibid.* **90**, 030403 (2003).
- [6] A. Perrin *et al.*, *Phys. Rev. Lett.* **99**, 150405 (2007).
- [7] R. G. Dall *et al.*, *Phys. Rev. A* **79**, 011601(R) (2009).
- [8] K. M. Hilligsøe and K. Mølmer, *Phys. Rev. A* **71**, 041602(R) (2005); N. Gemelke *et al.*, *Phys. Rev. Lett.* **95**, 170404 (2005); G. K. Campbell *et al.*, *ibid.* **96**, 020406 (2006).
- [9] E. V. Goldstein and P. Meystre, *Phys. Rev. A* **59**, 1509 (1999).
- [10] H. Pu and P. Meystre, *Phys. Rev. Lett.* **85**, 3987 (2000); L.-M. Duan *et al.*, *ibid.* **85**, 3991 (2000).
- [11] J. P. Burke *et al.*, *Phys. Rev. A* **70**, 033606 (2004).
- [12] C. Klempt *et al.*, *Phys. Rev. Lett.* **103**, 195302 (2009).
- [13] J. Catani *et al.*, *Phys. Rev. A* **77**, 011603(R) (2008).
- [14] D. M. Weld *et al.*, *Phys. Rev. Lett.* **103**, 245301 (2009).
- [15] D. McKay and B. DeMarco, arXiv:0911.4143v1 [New J. Phys. **12**, 055013 (2010) (published)].
- [16] A. B. Kuklov and B. V. Svistunov, *Phys. Rev. Lett.* **90**, 100401 (2003); E. Altman *et al.*, *New J. Phys.* **5**, 113 (2003); A. Isacsson *et al.*, *Phys. Rev. B* **72**, 184507 (2005).
- [17] A. Recati *et al.*, *Phys. Rev. Lett.* **94**, 040404 (2005); P. P. Orth, I. Stanic, and K. Le Hur, *Phys. Rev. A* **77**, 051601(R) (2008).
- [18] P. Pedri *et al.*, *Phys. Rev. Lett.* **87**, 220401 (2001).
- [19] P. L. Gould, G. A. Ruff, and D. E. Pritchard, *Phys. Rev. Lett.* **56**, 827 (1986); Y. B. Ovchinnikov *et al.*, *ibid.* **83**, 284 (1999).
- [20] B. Gadway *et al.*, *Opt. Express* **17**, 19173 (2009).
- [21] D. Pertot *et al.*, *J. Phys. B* **42**, 215305 (2009).
- [22] M.-O. Mewes *et al.*, *Phys. Rev. Lett.* **78**, 582 (1997).
- [23] I. H. Deutsch and P. S. Jessen, *Phys. Rev. A* **57**, 1972 (1998); D. Jaksch *et al.*, *Phys. Rev. Lett.* **82**, 1975 (1999).
- [24] S. J. J. M. F. Kokkelmans (private communication); B. J. Verhaar, E. G. M. van Kempen, and S. J. J. M. F. Kokkelmans, *Phys. Rev. A* **79**, 032711 (2009).
- [25] F. Dalfovo *et al.*, *Rev. Mod. Phys.* **71**, 463 (1999).
- [26] D. S. Hall *et al.*, *Phys. Rev. Lett.* **81**, 1539 (1998); **81**, 1543 (1998); K. M. Mertes *et al.*, *ibid.* **99**, 190402 (2007).